

Design, synthesis, and antidiabetic evaluation of novel 1,3-di(1,3,4-oxadiazol-2-yl)benzene derivatives as potent pancreatic α -amylase inhibitors: In vitro and in silico approaches

Assiya Atif^{a*}, Mohamed Marghich^b, Nor Nabil^c, Abouelhaoul El Alami^a, Nour Elhouda Daoudi^{d,e}, Tarik Harit^f, Fatima Youssoufi^a, Mohammed Salah^c, Abdelali Bitar^b and Houssine Ait Sir^a

^aBioorganic Chemistry Team, Laboratory of Bioorganic Chemistry, Faculty of Sciences, Chouaib Doukkali University, 24000 El Jadida, Morocco

^bNutritional Physiopathology, Neurosciences and Toxicology Team, Laboratory of Anthropogenetic, Biotechnology and health, Faculty of Sciences, Chouaib Doukkali University, 24000 El Jadida, Morocco

^cMolecular Modelling and Spectroscopy Research Team, Faculty of Science, Chouaib Doukkali University, P.O. Box 20, 24000, El Jadida, Morocco

^dHigher Institute of Nursing Professions and Health Techniques, Oujda 60000, Morocco

^eLaboratory of Bioresources, Biotechnology, Ethnopharmacology and Health, Department of Biology, Faculty of Sciences, Mohammed First University, 60 000 Oujda, Morocco

^fLaboratory of Applied Chemistry and Environment–ECOMP, Faculty of Sciences, Mohammed First University, 60000 Oujda, Morocco

CHRONICLE

Article history:

Received April 2, 2025

Received in revised form

June 10, 2025

Accepted September 14, 2025

Available online

September 14, 2025

Keywords:

Synthesis

Molecular docking

Molecular dynamics

Diabetes

α -amylase

ABSTRACT

The synthesis of a new family of 1,3-di(1,3,4-oxadiazol-2-yl)benzene derivatives is reported. Their structures were characterized using standard spectroscopic techniques such FT-IR, ¹H-NMR, ¹³C-NMR spectroscopies and mass spectrometry. The antidiabetic potential of these synthetic molecules was evaluated by determining their *in vitro* inhibitory activity against pancreatic α -amylase enzymes. In addition, *in silico* molecular docking and pharmacokinetic simulations were performed to examine the compounds binding interactions with the enzyme active site and to assess their ADMET properties. Compared the used positive control, the obtained results show that all 1,3-di(1,3,4-oxadiazol-2-yl)benzene derivatives demonstrated a good potency to inhibit the α -amylase enzyme, Especially, the 2,2'-(1,3-phenylenebis(1,3,4-oxadiazole-5,2-diyl))dianiline (**5d**) with IC₅₀ of 0.393 mg/mL. Furthermore, the experimental findings were supported by molecular dynamics, docking and ADMET studies. The obtained data emphasizes compound **5d** as potential as safe and effective therapeutic agents targeting the pancreatic α -amylase enzyme.

© 2026 by the authors; licensee Growing Science, Canada.

1. Introduction

Heterocycle chemistry is a very broad field, given the number of heterocyclic compounds listed and which continues to expand¹⁻⁷. Heterocycles are cyclic organic molecules containing at least one non-carbon atom such as nitrogen or oxygen. These compounds are vital in various scientific domains, especially medicinal chemistry and biochemistry⁸⁻¹⁶. They are characterized by rings composed of different elements, are commonly found in natural products and are essential for biological processes. Their importance is particularly evident in the pharmaceutical industry, where over 90% of new drugs incorporate heterocyclic structures¹⁷. These compounds display a broad spectrum of biological activities, including antimicrobial¹⁸, anti-inflammatory¹⁹, antiviral²⁰, anti-Alzheimer²¹, anticancer²², vasorelaxant²³ and antidiabetic effects²⁴. This latter is characterized by chronic hyperglycemia²⁵, which disrupts normal metabolism and can lead to various serious complications such as neuropathy, retinopathy, nephropathy, and cardiopathy²⁶. Therefore, it is necessary to manage diabetes, and this management involves several mechanisms, including the use of products that stimulate insulin secretion and promote the transcription of proteins that act as receptors at the cellular level, thus allowing glucose to enter the cells. Other mechanisms, such as delaying intestinal absorption, are also involved in this management²⁷. Furthermore, An important strategy in the management of diabetes mellitus aims to intercept carbohydrate digestion by inhibiting enzymes

* Corresponding author

E-mail address assia.atif@gmail.com (A. Atif)

that aid in sugar breakdown, such as amylase and glucosidase²⁸. In fact, these mechanisms do not only help control blood sugar levels but also prevent the rapid development of long-term complications. The α -amylase enzyme plays a crucial role in the breakdown and absorption of glucose, making it a key focus for controlling postprandial hyperglycemia²⁹. In fact, there is two key forms of α -amylase: Salivary amylase, produced by the salivary glands, and pancreatic amylase, produced by the pancreas and released into the intestine, breaks down the 1,4-glycosidic bonds in oligosaccharides, converting them into oligosaccharides and disaccharides within the intestinal lumen³⁰. To inhibit this enzymatic process, Synthetic drugs such as acarbose, voglibose, and miglitol are commonly used. However, these drugs often cause side effects, particularly gastrointestinal disturbances and other health issues³¹. As a result, there is increasing interest in exploring alternative synthetic compounds, specifically those based on heterocyclic structures, due to their potential efficacy and reduced side effect profiles.

Oxadiazole derivatives are a family of N,O-heterocyclic compounds with high biological values³². The literature reports several compounds endowing such heterocycle with good antibacterial³³, antitumor³⁴, anti-inflammatory potencies³⁵. Medicinal chemistry is concerned with the discovery, development, identification, and interpretation of the mode of action of biologically active compounds at the molecular level. 1,3,4-Oxadiazole derivatives have emerged as a potential option for antidiabetic drug research. 1,3,4-Oxadiazole derivatives have demonstrated the ability to improve glucose tolerance, enhance insulin sensitivity, and reduce fasting blood glucose levels³⁶, we set an example by : 5-(furan-2-yl)-3-((p-tolylamino)methyl)-1,3,4-oxadiazole-2(3H)-thione (**1**) has moderate to excellent antidiabetic activity, showing no negative impact on productivity at an oral dose of 40 mg/kg³⁷ and 3-(5-((2-amino-6-nitrophenyl)thio)-1,3,4-oxadiazol-2-yl)-8-bromo-2H-chromen-2-one (**2**) which showed strong inhibition of α -amylase³⁸.

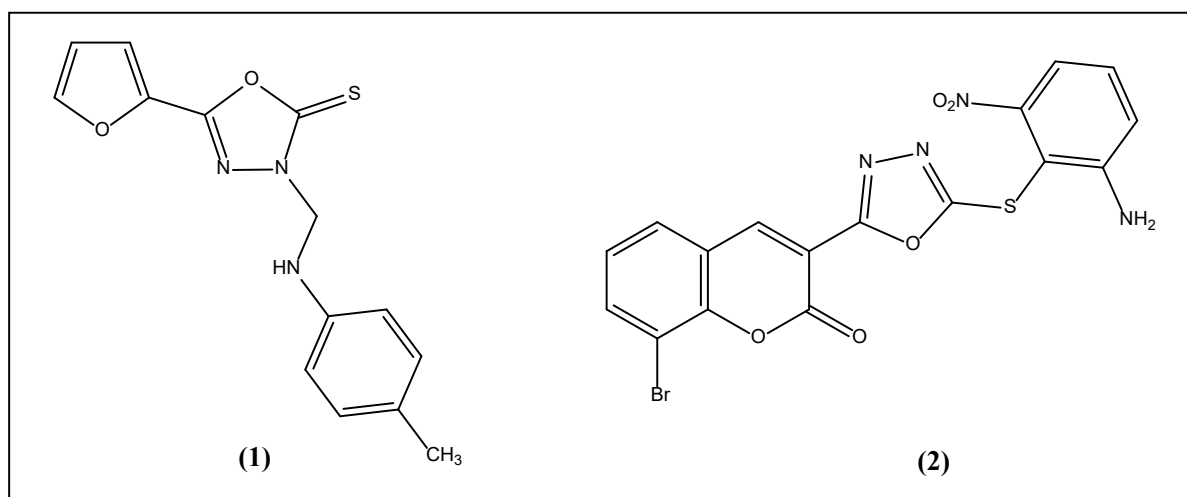


Fig. 1. Structure of compounds 1 and 2.

In this context, a new family of 1,3-di(1,3,4-oxadiazol-2-yl)benzene derivatives were synthesized to elucidate their antidiabetic potential by evaluating their *in vitro* inhibitory activity against α -amylase. Additionally, we conducted comprehensive *in silico* molecular docking, molecular dynamics and, Pharmacokineticsimulations to investigate the binding interactions of these compounds within the active sites of the α -amylase enzyme and examined their absorption, distribution, metabolism, excretion and toxicity.

2. Materials and Methods

2.1. Reagents and instruments

All reagents and solvents were obtained from Sigma Aldrich and used as received. Reaction progress is monitored by thin-layer chromatography (TLC) on aluminum sheets coated with Merck 60 F254 silica gel (thickness 0.2 mm) using the mobile phase (ethanol/ethyl acetate, 1:1). Revelation is carried out under a UV-Visible lamp (at 254 and 365 nm). The melting points of the synthesized compounds were determined using a Köfler bench and are not corrected to degrees Celsius. FTIR spectra were recorded on a SHIMADZU FT-IR 8400S spectrometer with a Smart iTR accessory and attenuated with total reflection crystal diamond (ATR) in the range (500-4000 cm^{-1}). Spectra were recorded on a Fourier transform JNM-ECZ500/S1 FT NMR SYSTEM (JEOL) (500 MHz for proton and 125 MHz for carbon 13) at the Centre National pour la Recherche Scientifique et Technique (CNRST) in Rabat. High-resolution mass spectrometry (HRMS) was performed using an Ultimate 3000-Exactive Plus Thermo quadrupole-Orbitrap mass spectrometer, equipped with a collision cell, also housed at the CNRST in Rabat.

2.2. Synthesis

2.2.1. Synthesis of dimethyl isophthalate (2)

Esterification of isophthalic acid involves reacting the acid (**1**) (7 mmol) with a mixture of thionyl chloride SOCl_2 (8 mL) and methanol (30 mL) at reflux for 24 hours. After the reaction, the mixture is neutralized using 10% NaHCO_3 , giving white crystals which are separated by filtration, washed and recrystallized in methanol^{39,40}. White crystal, m.p 68°C; yield 90%. ^1H NMR (500MHz/DMSO- d_6 ,ppm): 3.86(s,6H,OCH₃), 7.21(s,1H,CHar), 7.36(d,2H,CHar), 7.79(t,1H,CHar), ^{13}C NMR (125MHz/DMSO- d_6 , ppm) : 162.86(2C=O), 134.41(2Car), 131.28(2Car), 128.79(Car), 127.30(Car), 56.56(2OCH₃), IR (cm^{-1}): 1625 $\nu\text{C}=\text{O}$, 1279 $\nu\text{O}-\text{CH}_3$

2.2.2. Synthesis of isophthalohydrazide (3)

Isophthalohydrazide (**3**) was prepared from dimethyl isophthalate (**2**) (7 mmol) and excess hydrazine hydrate (10 mL) under magnetic stirring at room temperature for 18 hours. Hydrazine hydrate was removed by the addition of methanol, then filtered through a büchner. The white solid was then recrystallized in ethanol⁴¹. White solid, m.p 227°C; yield 88%. ^1H NMR (500MHz/DMSO- d_6 ,ppm): 4.82(s,4H,NH²), 7.21(s,1H,CHar), 7.39(d,2H,CHar), 7.79(t,1H,CHar), 9.32(s,2H,NH), ^{13}C NMR (125MHz/DMSO- d_6 , ppm) : 168.10(2C=O), 132.44(Car), 131.07(2Car), 130.16(2Car), 128.32(Car), IR (cm^{-1}): 1721 $\nu\text{C}=\text{O}$, 3052-3108 νNH_2 , 3209 $\nu\text{N}-\text{H}$

2.2.3. General method for the synthesis of 1,3-di(1,3,4-oxadiazol-2-yl)benzene derivatives (5)

1,3,4-oxadiazole derivatives are obtained by reacting (6 mmol) acid (**4**) and (3 mmol) isophthalohydrazide (**3**) in the presence of phosphoryl trichloride (15 mL) at reflux for 6 hours. After neutralizing the reaction mixture with 25% ammonia to pH=7, a solid is obtained which has been filtered, washed and recrystallized in ethanol⁴²⁻⁴⁴.

1,3-Bis(5-(4-methoxyphenyl)-1,3,4-oxadiazol-2-yl)benzene (5a). yield 89%, m.p 121°C, ^1H NMR (500MHz/DMSO- d_6 ,ppm): 3.33(s,6H,OCH₃), 7.39(d,4H,CHar), 7.47(d,4H,CHar), 7.55(s,1H,CHar), 7.82(t,1H,CHar), 8.07(d,2H,CHar), ^{13}C NMR (125MHz/DMSO- d_6 , ppm) : 161.46(4C=N), 160.60(2Car), 130.54(Car), 130.16(2Car), 128.79(2Car), 127.30(2Car), 126.44(Car), 117.53(4Car), 115.51(4Car), 69.00(2OCH₃), IR (cm^{-1}): 1629 $\nu\text{C}=\text{N}$, 1293 $\nu\text{C}-\text{O}$, MS(ESI): m/z = 427 [M+H]⁺

1,3-Bis(5-(thiophen-2-yl)-1,3,4-oxadiazol-2-yl)benzene (5b). yield 69%, m.p 147°C, ^1H NMR (500MHz/DMSO- d_6 ,ppm): 8.00(d,2H,CHar), 8.06(d,2H,CHar), 8.26(t,2H,CHar), 8.34(s,1H,CHar), 8.35(d,2H,CHar), 8.62(t,1H,CHar), ^{13}C NMR (125MHz/DMSO- d_6 , ppm) : 162.86(4C=N), 133.55(2Car), 132.44(2Car), 130.08(Car), 128.89(2Car), 128.06(2Car), 127.30(2Car), 126.44(2Car), 124.53(Car), IR (cm^{-1}): 1612 $\nu\text{C}=\text{N}$, MS(ESI): m/z = 379 [M+H]⁺

4,4'-(1,3-Phenylenebis(1,3,4-oxadiazole-5,2-diyl))bis(benzene-1,2-diamine) (5c). yield 62%, m.p >300°C, ^1H NMR (500MHz/DMSO- d_6 ,ppm): 6.48(s,4H,NH₂), 6.51(s,4H,NH₂), 7.18(s,2H,CHar), 7.24(d,2H,CHar), 7.27(d,2H,CHar), 7.68(s,1H,CHar), 7.82(d,2H,CHar), 7.88(t,1H,CHar), ^{13}C NMR (125MHz/DMSO- d_6 , ppm) : 162.86(4C=N), 136.44(2Car), 134.75(2Car), 130.54(Car), 128.37(2Car), 127.60(2Car), 126.44(Car), 117.53(2Car), 116.41(2Car), 115.32(2Car), 114.79(2Car), IR (cm^{-1}): 3122-3217 νNH_2 , 1625 $\nu\text{C}=\text{N}$, MS(ESI): m/z = 427 [M+H]⁺

2,2'-(1,3-Phenylenebis(1,3,4-oxadiazole-5,2-diyl))dianiline (5d). yield: 84%, m.p 227°C, ^1H NMR (500MHz/DMSO- d_6 ,ppm): 6.38(s,4H,NH₂), 7.10(t,2H,CHar), 7.18(d,2H,CHar), 7.23(t,2H,CHar), 7.39(d,2H,CHar), 7.49(d,2H,CHar), 7.64(s,1H,CHar), 7.79(t,1H,CHar), 8.07(t,1H,CHar), ^{13}C NMR (125MHz/DMSO- d_6 , ppm) : 168.10(4C=N), 146.80(2Car), 130.64(Car), 130.16(2Car), 128.79(2Car), 127.83(2Car), 126.54(2Car), 124.53(Car), 121.62(2Car), 117.53(2Car), 114.79(2Car), IR (cm^{-1}): 3154-3201 νNH_2 , 1670 $\nu\text{C}=\text{N}$, MS(ESI): m/z = 397 [M+H]⁺

1,3-Bis(5-(pyridin-2-yl)-1,3,4-oxadiazol-2-yl)benzene (5e). yield: 77%, m.p 205°C, ^1H NMR (500MHz/DMSO- d_6 ,ppm): 7.06(d,2H,CHar), 7.10(t,2H,CHar), 7.21(t,2H,CHar), 7.49(d,2H,CHar), 7.52(s,1H,CHar), 7.78(t,1H,CHar), 7.83(d,2H,CHar), ^{13}C NMR (125MHz/DMSO- d_6 , ppm) :169.06(4C=N), 156.66(2Car), 148.35(2Car), 136.44(2Car), 128.79(Car), 127.83(2Car), 126.44(2Car), 124.53(Car), 121.62(2Car), 120.80(2Car), IR (cm^{-1}): 1736 $\nu\text{C}=\text{N}$, MS(ESI): m/z = 369 [M+H]⁺

2.3. In Vitro, pancreatic α -amylase inhibition

The experimental mixtures included 200 μL of porcine pancreatic α -amylase enzyme solution (13 IU), 200 μL of phosphate buffer (0.02 M; pH = 6.9), and 200 μL of 1,3-di(1,3,4-oxadiazol-2-yl)benzene derivatives at specific concentrations (**0.11**, **0.22**, **0.45**, **0.9 mg/mL**). The mixtures were pre-incubated at 37 °C for 10 minutes. Subsequently, 200 μL of starch (1%) dissolved in phosphate buffer solution was added to each tube and incubated for 20 minutes at 37 °C. Subsequently, 600 μL of 3,5-dinitrosalicylic acid (ADNA) dye reagent was incorporated to terminate the enzymatic reaction. Subsequently, the tubes were incubated for 8 minutes at a temperature of 100 °C. Subsequently, they were immersed in a cold water bath for a few minutes. The absorbance was determined at 540 nm after diluting the mixture by adding 1 ml of

distilled water³⁰. All assays were performed in triplicate. The formula below was used to calculate the percentage inhibition :

$$\text{Inhibitory activity (\%)} = \frac{\text{OD Control} - \text{OD Test}}{\text{OD Control}} \times 100$$

The concentration of the samples inhibiting the enzymatic activity of α -amylase by 50% (IC₅₀) was calculated graphically according to the function:

Inhibition percentage = f (log sample concentration)

2.4. Molecular docking study

The docking study was carried out using “iGemdock program”⁴⁵. The 3D structure of porcine pancreatic alpha-amylase complexed with acarbose (1OSE) was extracted from the Protein Data Bank (<https://www.rcsb.org/>). The 3D structure of compounds **L**₁-**L**₃ was optimized using Chem3D Ultra 8.0. The binding energy was determined using the following equation: Binding Energy = Van der Waal’s (V) energy + hydrogen-bonding (H) energy + electrostatic (E) energy. The used parameters during the calculations were: population size: 200; generations: 70; solutions: 3 (Drug screening). The 2D docked poses were displayed BIOVIA Discovery Studio Visualizer 2021 v21.1.0.20298 (<https://discover.3ds.com/discovery-studio-visualizer-download>), respectively.

2.5. In silicopredicting of the pharmacokinetics and Toxicity of the molecules

Pharmacokinetics *Properties* of the molecules were evaluated *in silico* using computational tools available on the SwissADME online server (<http://www.swissadme.ch/>, accessed on July 27, 2024)⁴⁶. The assessment of LD₅₀ values, toxicity class, hepatotoxicity, carcinogenicity, immunotoxicity, mutagenicity, and cytotoxicity was conducted utilizing the Protox II online tool (https://tox-new.charite.de/protox_II/, accessed on December on July 27, 2024)⁴⁷. The ADME (Absorption, Distribution, Metabolism and Excretion) profiles were assessed *in silico* via pkCSM web-server (<http://biosig.unimelb.edu.au/pkcsml/>, accessed on July 27, 2024)⁴⁸.

2.6. Molecular dynamics study

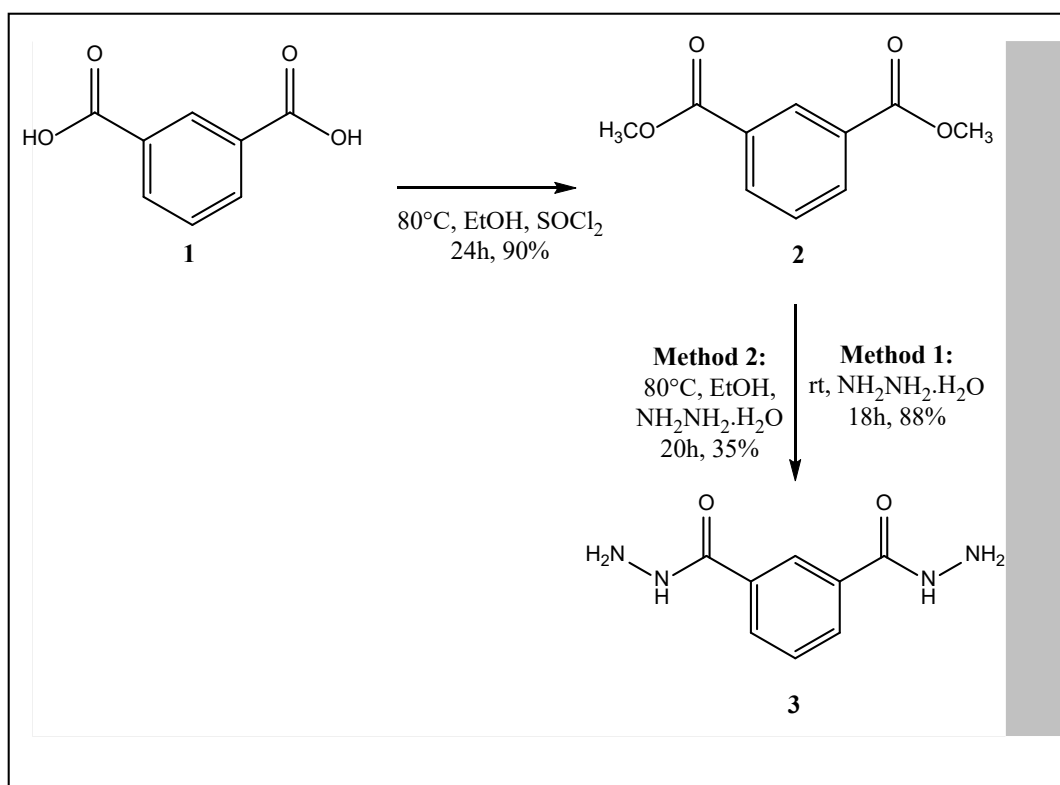
The molecular dynamics (MD) simulation workflow began with the preparation of the protein-ligand complex, wherein the three-dimensional structure was obtained and completed using the SwissDrugDesign protocol to correct any missing atoms or residues, ensuring a structurally sound input suitable for simulation. Ligand topology was subsequently generated via the CHARMM General Force Field (CGenFF) server, and the resulting files were converted into a GROMACS-compatible format using the cgenff_charmm2gmx.py script. The system was then preprocessed by generating molecular topology files using the GROMOS96 43a1 force field for the protein and CGenFF for the ligand. Solvation was performed in a Triclinic box with a minimum distance of 1.0 nm between the protein and box boundaries, using the Simple Point Charge (SPC) water model, while counterions (Na⁺ and Cl⁻) were added to neutralize the system and mimic physiological conditions at 0.15 M NaCl. Energy minimization was carried out using the steepest descent algorithm with a maximum of 5000 steps and a convergence criterion of 1000 kJ/mol/nm to eliminate steric clashes and optimize the initial structure. The system underwent two phases of equilibration: NVT (constant volume and temperature) using the V-rescale thermostat at 298 K for 100 ps, followed by NPT (constant pressure and temperature) using the Berendsen barostat at 1.0 bar for 100 ps, both with a 2 fs time step, ensuring thermodynamic stability before production simulation. The production MD run was conducted for 50 ns and 100 ns using the Leap-frog integrator, employing periodic boundary conditions in all directions, a 2 fs time step, and recording 1000 frames, with long-range electrostatics handled via the Particle Mesh Ewald (PME) method and a 1.0 nm cutoff for both van der Waals and electrostatics interactions. Upon completion, trajectory analysis was performed to assess system behavior through several metrics: Root Mean Square Deviation (RMSD) to monitor structural stability over time, Root Mean Square Fluctuation (RMSF) to evaluate residue-level flexibility, Radius of Gyration (Rg) to analyze the protein’s compactness, Solvent Accessible Surface Area (SASA) to gauge the exposure of residues to the solvent, and the number of hydrogen bonds formed to investigate protein-ligand interactions, collectively providing a comprehensive understanding of the structural dynamics and stability of the complex throughout the simulation.

3. Results and Discussion

3.1. Synthesis of 1,3-di(1,3,4-oxadiazol-2-yl)benzene derivatives (**5a-5e**)

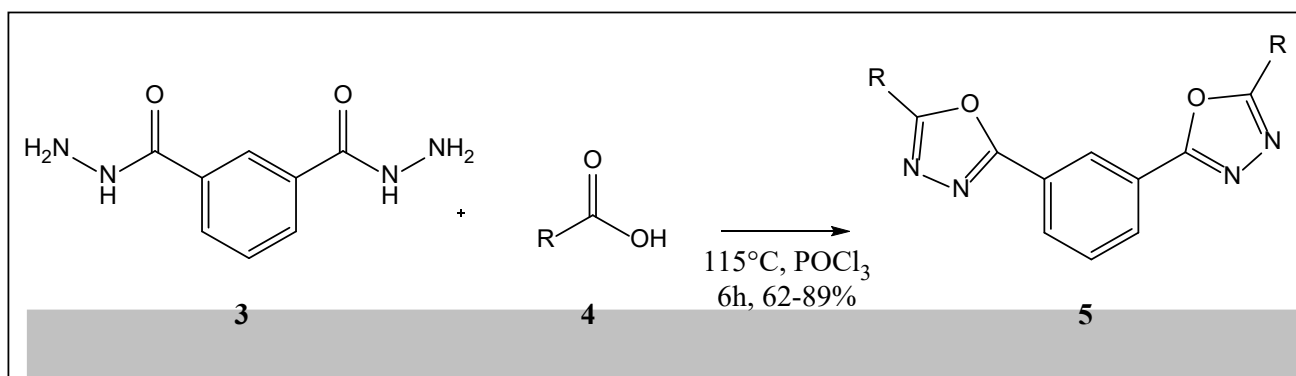
A mixture of thionyl chloride and methanol is added to isophthalic acid (**1**) at reflux for 24 hours, leading to the corresponding diester (**2**)³⁹⁻⁴⁰, we utilized thionyl chloride as a catalyst for the esterification reaction, which significantly improved yields compared to traditional esterification in methanol with H₂SO₄. This approach ensured complete consumption of the starting acids within an optimized reaction time. Two methods of producing isophthalohydrazide(**3**) were followed. In the first route, diester (**2**) was reacted with excess hydrazine hydrate in ethanol at reflux for 20 hours, yielding product (**3**) in less than 35% yield. In the second route, the same substrate was simply reacted with excess hydrazine hydrate at room temperature for 18 hours, giving the desired compound (**3**) in 88% yield. **Scheme (1)**. In this step, unlike

the conventional reflux method used in most studies including the work of Amirand Shikha, (2004)⁴⁹, we carried out the acid hydrazide formation at room temperature, which gave excellent yields. Moreover, unlike the work of Li et al., (2008)⁵⁰, where the reaction was carried out under reflux conditions, we opted for a solvent-free reaction at room temperature, which increased the yield up to 88%.



Scheme 1. Procedure for synthesis of isophthalohydrazide (3).

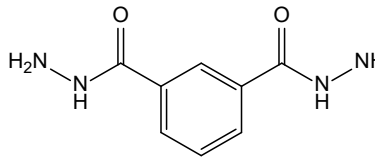
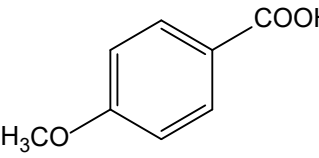
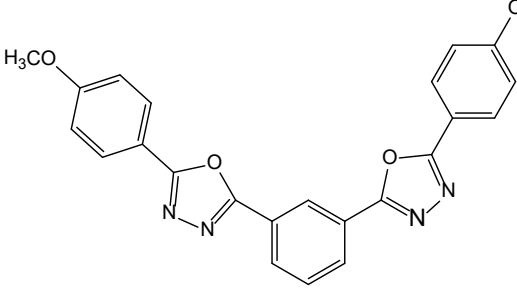
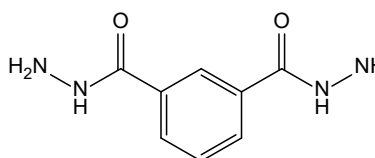
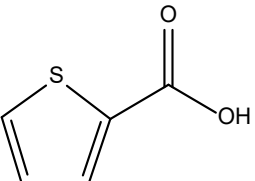
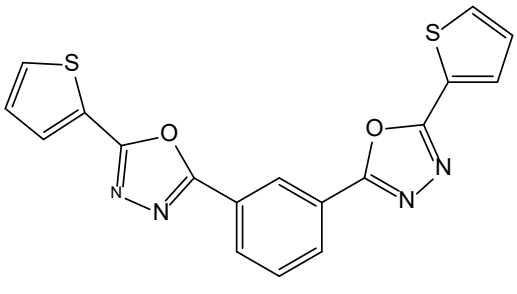
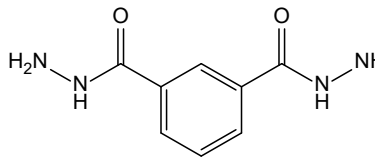
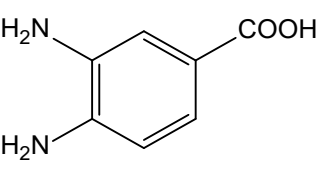
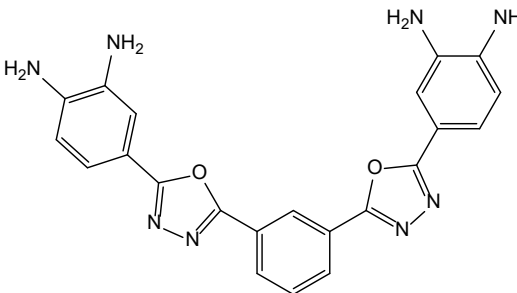
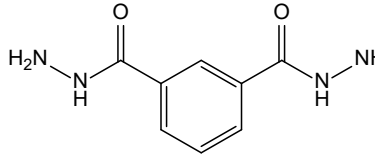
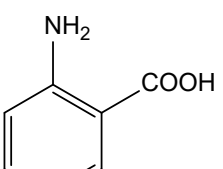
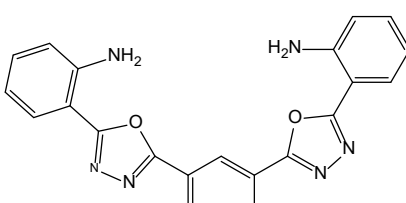
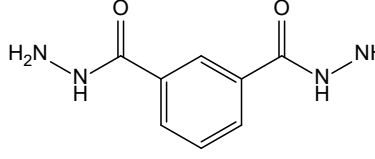
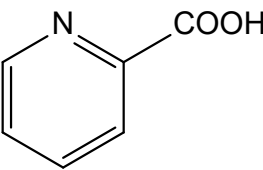
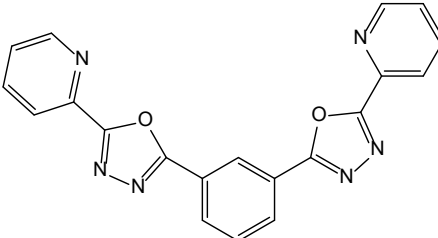
Different methods have been cited in the literature⁵¹⁻⁵², in our work, the synthesis of bis-1,3,4-oxadiazole derivatives (5) is supported by the use of phosphoryl trichloride by condensing acid hydrazide (3) with carboxylic acid derivatives (9)⁴²⁻⁴⁴. Scheme (2). In this third step, we synthesized new oxadiazole derivatives under optimized conditions, reaching yields ranging from 62% to 90%, different from the compounds previously reported in the literature.



Scheme 2. Synthesis of 1,3-di(1,3,4-oxadiazol-2-yl)benzene derivatives.

Resulting 4,4'-(1,3-phenylenebis(1,3,4-oxadiazole-5,2-diyl))bis(benzene-1,2-diamine) was subjected to ^1H NMR, ^{13}C NMR, IR and mass spectrometry. ^1H NMR spectrum shows two signals at 6.48 and 6.51 ppm attributable to amine protons, and signals attributable to benzene protons between 7.18 ppm and 7.88 ppm. ^{13}C NMR spectrum highlights, in particular, four $\text{C}=\text{N}$ bond signals at 162.86 and signals at 136.44, 134.75, 130.54, 128.37, 127.60, 126.44, 117.53, 116.41, 115.32 and 114.79 ppm attributable to benzene carbons. IR spectroscopy revealed two absorption bands at $3122\text{-}3217\text{ cm}^{-1}$ for NH_2 groups and a band at 1625 cm^{-1} for the $\text{C}=\text{N}$ bond. The compound's ESI mass spectrum shows a molecular peak at $m/z = 427\text{ [M+H]}^+$.

Table 1. 1,3-di(1,3,4-oxadiazol-2-yl)benzenederivatives.

N°	Hydrazid	Acid	Compound structure
<u>1</u>			
<u>2</u>			
<u>3</u>			
<u>4</u>			
<u>5</u>			

The following formula used for the calculation of the yield of the synthetic molecules:

$$\text{yield (\%)} = \frac{\text{experimental mass}}{\text{theoretical mass}} \times 100$$

Our reported yields (ranging from 62% to 89%). Furthermore, when compared to previously published studies on the synthesis of 1,3,4-oxadiazole derivatives, our yields are quite competitive and, in many cases, superior. For instance, Jha et al., (2010)⁵² synthesized similar derivatives using phosphoryl trichloride (POCl₃) and obtained yields of 97%, 75%, 59%, 60%, and 68%. Using carbon disulfide (CS₂), their yields were 79%, 64%, 58%, 62%, and 71%. Ziga and Dolec (2008)⁵³

reported yields of 81%, 71%, 63%, 69%, and 68% using POCl₃, while their alternative methodology involving CDI, PPh₃, and CBr₄ led to significantly lower yields (52%, 66%, 73%, 23%, and 0%). Yadav et al., (2016)⁵⁴ also used POCl₃ and obtained yields of 61%, 64%, and 67%. Given these comparisons, our results demonstrate a favorable efficiency in the synthesis of 1,3,4-oxadiazole derivatives.

3.2. *In Vitro*, pancreatic α -amylase inhibition of 1,3-di(1,3,4-oxadiazol-2-yl)benzene derivatives

The therapeutic potential of drug derivatives is assessed through their IC₅₀ values, drug-receptor interactions, and *in vitro* activity profiles⁵⁵. Therefore, the molecules were assessed for their inhibitory activity against α -amylase enzymes. Both **5d** and **5b** demonstrated a dose-dependent inhibition, showing significant efficacy compared to the control. Particularly **5d** pronounced a great activity against α -amylase, exhibiting inhibitions of 26.81%, 47.29%, and 72.61% at concentrations of 0.22, 0.45, and 0.9 mg/mL, respectively, followed by **5b**. In comparison, the reference drug acarbose exhibited inhibitions of 59.59%, 67.07%, and 77.80% at the same concentrations (**Fig. 2**). These findings indicate that **5d** and **5b** elicited effects comparable to those of acarbose, this conclusion supported by the IC₅₀ values: **5d**, **5b** and acarbose had an IC₅₀ values of 0.393 ± 0.007, 0.503 ± 0.006, and 0.159 ± 0.008 mg/mL, respectively (**Table 2**). In addition, after using the maximum dose of 0.9 mg/mL, molecule **5d** demonstrated an effect comparable to acarbose, achieving **80%** of inhibition. In contrast, the other molecules exhibited inhibition effects ranging from 50% to 65%. These molecules as a great inhibitory effect on α -amylase than to other compounds like 5-amino-nicotinic acid derivatives⁵⁶, and a series of phosphoramidates containing a heterocyclic⁵⁷. Other new designed molecules like 1,3,5-trisubstituted-2-thioxoimidazolidin-4-ones⁵⁸ and 2-(3-(3-methoxybenzoyl)-4-hydroxy-1,1-dioxido-2H-benzo[e][1,2]thiazin-2-yl)-N-arylacetamides⁵⁹ exhibits a considerable inhibitory activity toward α -amylase.

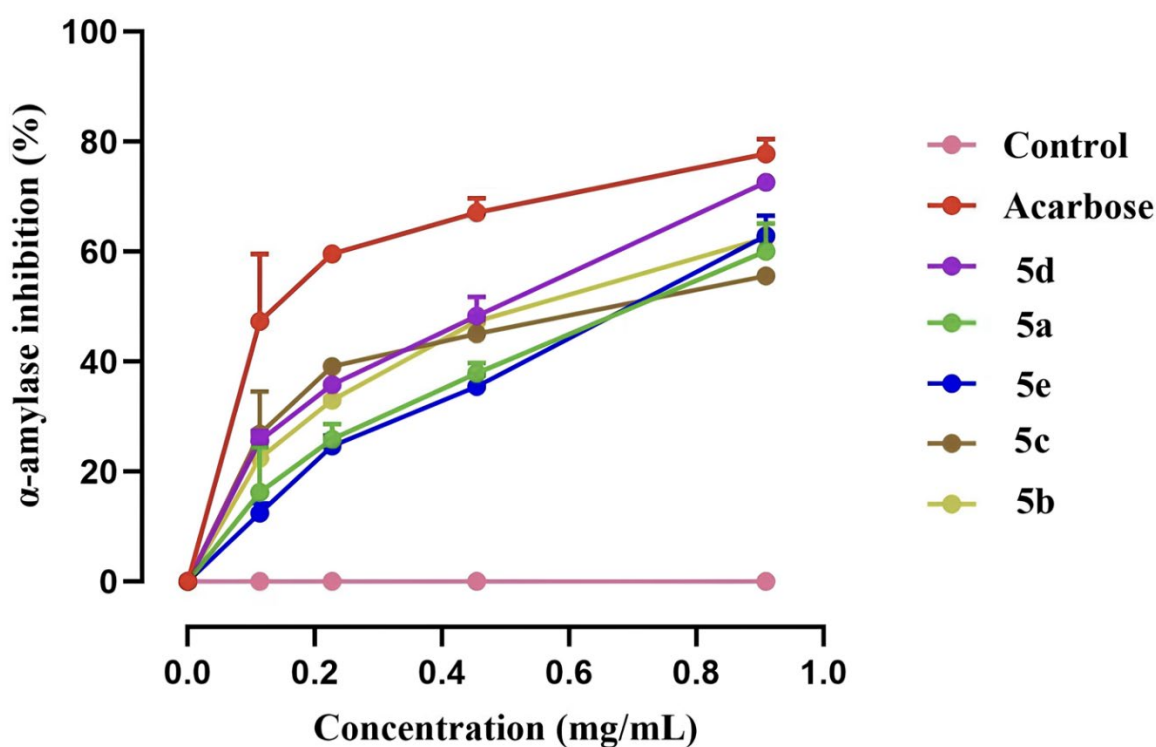


Fig 2. *In vitro* inhibition of the α -amylase activity by the 1,3-di(1,3,4-oxadiazol-2-yl)benzene derivatives (**5a**, **5b**, **5c**, **5d**, **5e**) and the acarbose (reference drug).

Table 2. IC₅₀ Value of the inhibition of α -amylase by the 1,3-di(1,3,4-oxadiazol-2-yl)benzene derivatives (**5a**, **5b**, **5c**, **5d**, **5e**) and the acarbose (reference drug).

	IC ₅₀ (mg/mL)
Acarbose	0.159 ± 0.008
5a	0.692 ± 0.080
5b	0.503 ± 0.006
5c	0.600 ± 0.032
5d	0.393 ± 0.007
5e	0.642 ± 0.016

To put light on the effect of the nature group attached to the oxadiazol ring on the α -amylase inhibition activity a structure activity relationship (SAR) was conducted. Compound **5a** with a methoxy group on the para position displays the

low potency. Replacing the *para*-methoxy phenyl fragment by the pyridine one (**5e**) slightly increases the activity of this compound. Furthermore, the substitution of the OCH₃ by NH₂ with additional NH₂ at the *meta* position (**5c**) also enhances the potency of this molecule in weak manner. This was also observed when the *para*-methoxy phenyl fragment was replaced by the thiophene ring (**5b**). Finally, the presence of the amino group in the *ortho* position (**5d**) improves the α -amylase inhibition potency to reach the best value among the five tested compounds.

3.3. Molecular docking study

The primary goal of any synthetic research is to identify candidates with biological activity. However, the process of synthesizing a multitude of organic compounds, followed by biological screening, is both time-consuming and expensive. *In silico* methods⁴⁵ can facilitate and optimize this process. We began our research by redocking acarbose, as outlined in our previous work⁶⁰. As illustrated in **Fig. 3**, the major residues involved correspond almost perfectly to those documented experimentally⁶¹, which therefore validates the docking protocol.

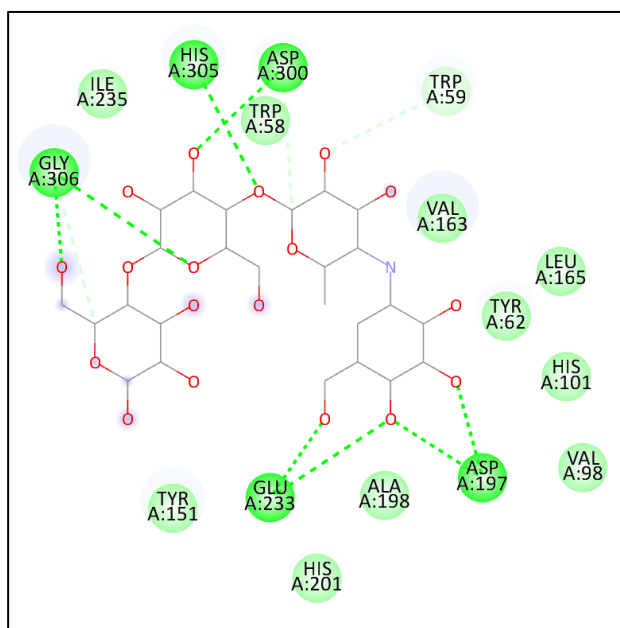


Fig. 3. Interactions of the active site residues with of Acarbose.

Subsequently, all molecules were subjected to the same docking procedure. **Fig. 4** illustrates the 2D binding configurations. Docking results with the pancreatic α -amylase enzyme revealed a highly preserved binding region, however the interactions between the ligand and the active site differ. Concerning the binding energy of the examined compounds increases in this order **5a**>**5e**>**5c**>**5b**>**5d**>Acarbose (**Table 3**). Another *in silico* study identified a thiazolidine-2,4-dione derivative (compound **7a**) as a promising α -amylase inhibitor with strong binding affinity, underscoring its potential therapeutic use in diabetes management⁶². Additionally, novel 1,2,3-triazole-linked coumarin and cinnamic acid analogs demonstrated significant *in silico* antidiabetic activity as potent α -amylase inhibitors, indicating their suitability for further pharmacological development⁶³. Furthermore, recent studies highlight the growing interest in synthetic compounds targeting α -amylase as effective strategies in diabetes management. For instance, research on tetrapodal compounds⁶⁴ has shown that these derivatives exhibit strong binding affinities to the α -amylase enzyme, reinforcing the idea that structure-activity relationships play a crucial role in the development of effective α -amylase inhibitors. This trend underscores the importance of exploring diverse synthetic frameworks to enhance the potency and efficacy of new antidiabetic agents. The results from the docking studies are consistent with the *in vitro* study findings. The compound **5e**, which showed the lowest IC₅₀ value (0.393 ± 0.007 mg/mL) among the synthesized derivatives, also demonstrated a relatively low binding energy (-124.7 Kcal/mol), suggesting a strong interaction with the active site of the pancreatic α -amylase enzyme. This aligns with the observed potent inhibitory activity. On the other hand, compounds such as **5b**, which exhibited a higher IC₅₀ value (0.692 ± 0.080 mg/mL), correspondingly showed a higher binding energy (-112.2 Kcal/mol).

3.4. Pharmacokinetic and ADMET Properties of the novel 1,3-di(1,3,4-oxadiazol-2-yl)benzene derivatives (**5a**, **5b**, **5c**, **5d**, **5e**)

Table 4 evaluates five 1,3-di(1,3,4-oxadiazol-2-yl)benzene derivatives (**5a**, **5b**, **5c**, **5d** and **5e**) using various drug-likeness and bioavailability filters, including Lipinski's Rule of Five, Ghose, Veber, Egan, and the Bioavailability Score. **5d**, **5b**, **5c**, and **5e** fully adhere to Lipinski's Rule with no violations. However, **5a** breaches this rule in one aspect: its MLOGP (logarithm of partition coefficient) exceeds 4.15. **5a** also fails to meet Ghose's filter due to its WLOGP value surpassing 5.6, indicating excessive lipophilicity. The other compounds successfully pass Ghose's filter. Concerning the

Veber rule, **5c** is non-compliant because its Topological Polar Surface Area (TPSA) exceeds 140, implying potential issues with absorption, while the other compounds meet the requirements. As for the Egan rule, **5b** and **5c** violate the criteria due to TPSA values exceeding 131.6, whereas the other compounds comply. Finally, all compounds have a bioavailability index of 0.55, meaning overall average bioavailability. This score confirms the good absorption after oral administration of these compounds⁶⁵.

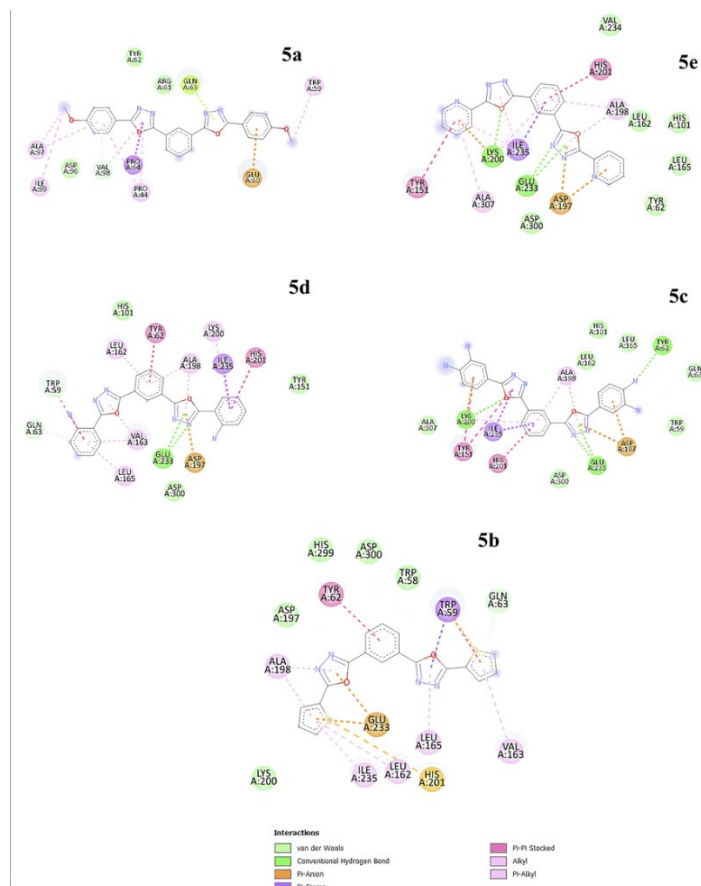


Fig 4. 2D interactions of the active pocket residues with molecules **1,3-di(1,3,4-oxadiazol-2-yl)benzene derivatives (5a, 5b, 5c, 5d, 5e)**.

Table 3. Binding energies of novel **1,3-di(1,3,4-oxadiazol-2-yl)benzene derivatives (5a, 5b, 5c, 5d, 5e)** and the acarbose (reference drug).

	Binding energy(Kcal/mol)
Acarbose	-125.8
5a	-112.2
5b	-120.7
5c	-115.7
5d	-124.7
5e	-113.4

Table 4. Drug likeness and bioavailability score in *silico* prediction of novel **1,3-di(1,3,4-oxadiazol-2-yl)benzene derivatives (5a, 5b, 5c, 5d, 5e)**.

	5d	5a	5b	5c	5e
Lipinski	Yes	Yes; 1 violation: MLOGP>4.15	Yes	Yes	Yes
Ghose	Yes	No; 1 violation: WLOGP>5.6	Yes	Yes	Yes
Veber	Yes	Yes	Yes	No; 1 violation: TPSA>140	Yes
Egan	Yes	Yes	No; 1 violation: TPSA>131.6	No; 1 violation: TPSA>131.6	Yes
Bioavailability Score	0.55	0.55	0.55	0.55	0.55

Table 5 presents key properties of five novel 1,3-di(1,3,4-oxadiazol-2-yl)benzene derivatives (**5a**, **5b**, **5c**, **5d** and **5e**) related to water solubility, permeability, absorption, and their interactions with the P-glycoprotein (P-gp) transporter system. All compounds display poor water solubility and limited skin permeability, highlighting potential challenges for formulation and minimal likelihood of dermal absorption. In terms of Caco-2 permeability, compounds **5e**, **5b**, and **5a** exhibit the highest permeability values, all exceeding 0.9, indicating a strong potential for intestinal absorption. In contrast, **5d** and **5c** have permeability values below 0.9, suggesting a reduced ability to pass through the intestinal barrier. Despite variations in permeability, all compounds show high intestinal absorption, with absorption rates greater than 30%, suggesting they are likely to be well absorbed when administered orally. Notably, **5c** is the only compound that serves as a substrate for P-gp, meaning it may be actively transported by this efflux pump, potentially affecting its distribution and bioavailability. The other compounds inhibit P-gp I and II, which could lead to drug interactions by influencing the P-gp-mediated transport of other substances.

Table 5. *In silico* Absorption prediction of novel 1,3-di(1,3,4-oxadiazol-2-yl)benzene derivatives (**5a**, **5b**, **5c**, **5d** and **5e**).

Unit	Water solubility Log mol/L	Caco2 permeability Log Papp in 10 ⁻⁶ cm/s	Intestinal absorption % Absorbed	Skin Permeability log Kp	P-gp substrate	P-gp I inhibitor	P-gp II inhibitor
5d	-3.102	0.292	100	-2.735	No	Yes	Yes
5a	-3.382	1.096	98.866	-2.735	No	Yes	Yes
5b	-3.179	1.153	93.316	-2.735	No	Yes	Yes
5c	-3.153	0.108	83.754	-2.735	Yes	No	Yes
5e	-2.862	1.894	100	-2.735	No	Yes	Yes

The **table 6** provides pharmacokinetic data for novel 1,3-di(1,3,4-oxadiazol-2-yl)benzene derivatives (**5a**, **5b**, **5c**, **5d** and **5e**) related to their volume of distribution at steady state (VD_{ss}), fraction unbound (F_u), blood-brain barrier (BBB) permeability, and central nervous system (CNS) permeability. **5e** shows the highest tissue distribution (VD_{ss}), while **5c** is primarily confined to the plasma. **5a** has the highest unbound fraction and the greatest potential to cross the blood-brain barrier and penetrate the CNS, although still somewhat limited. In contrast, **5c** and **5e** exhibit poor CNS permeability and low BBB permeability, suggesting they are less likely to affect or reach the brain.

Table 6. Distribution characteristics prediction of novel 1,3-di(1,3,4-oxadiazol-2-yl)benzene derivatives (**5a**, **5b**, **5c**, **5d** and **5e**).

Unit	VD _{ss} (human) log L/kg	Fraction unbound (human) F _u	BBB permeability log BB	CNS permeability log PS
5d	-0.147	0.255	-1.095	-2.197
5a	0.193	0.316	-0.884	-1.731
5b	-0.1	0.3	-1.191	-2.001
5c	-0.621	0.147	-1.584	-2.558
5e	0.421	0.284	-1.336	-3.09

Table 7 provides data on the interactions of novel 1,3-di(1,3,4-oxadiazol-2-yl)benzene derivatives (**5a**, **5b**, **5c**, **5d** and **5e**) with various cytochrome P450 (CYP) enzymes. All compounds are substrates for CYP3A4, highlighting the enzyme's key role in their metabolism and their susceptibility to interactions with drugs that influence CYP3A4 activity. Additionally, all compounds inhibit CYP1A2, raising the potential for significant drug-drug interactions with medications metabolized by this enzyme. Notably, **5c** inhibits both CYP2D6 and CYP2C19, indicating a higher risk of complex drug interactions. **5e** is distinct in its inhibition of CYP3A4, potentially affecting the metabolism of a wide range of drug.

Table 7. *In silico* Metabolism parameter prediction of novel 1,3-di(1,3,4-oxadiazol-2-yl)benzene derivatives (**5a**, **5b**, **5c**, **5d** and **5e**).

	CYP2D6 substrate	CYP3A4 substrate	CYP1A2 inhibitor	CYP2C19 inhibitor	CYP2C9 inhibitor	CYP2D6 inhibitor	CYP3A4 inhibitor
5d	No	Yes	Yes	No	Yes	No	No
5a	No	Yes	Yes	No	Yes	No	No
5b	No	Yes	Yes	Yes	Yes	No	No
5c	No	Yes	Yes	Yes	Yes	Yes	No
5e	No	Yes	Yes	No	Yes	No	Yes

Table 8 presents data on the total clearance and renal OCT2 substrate classification novel 1,3-di(1,3,4-oxadiazol-2-yl)benzene derivatives (**5a**, **5b**, **5c**, **5d** and **5e**). **5a** has the highest total clearance, indicating rapid elimination, while **5c** has the lowest, suggesting prolonged retention in the body. **5e** is unique in its reliance on the renal OCT2 pathway, which could affect its elimination and increase the risk of interactions with drugs that influence OCT2 function. The remaining compounds are cleared through mechanisms independent of OCT2, suggesting fewer interactions related to this transporter.

The LD₅₀ values reflect the dose at which each substance is lethal to 50% of Rodent. A lower LD₅₀ value indicates higher acute toxicity. **5b** and **5a** have the lowest LD₅₀ values (888 mg/Kg), indicating they are the most toxic, while **5c** has the highest LD₅₀ (2035 mg/Kg) with the toxicity class of 5, suggesting it is the least toxic among the five substances (**Table 9**).

Regarding the toxicity profiles of these molecules, the results indicate that all substances exhibit a neurotoxicity, hepatotoxicity, and have the potential to cause cancer. Concerning the Respiratory Toxicity, **5d**, **5b**, and **5c** show active respiratory toxicity, while **5a** and **5e** are inactive. This suggests that **5a** and **5e** have no toxic effect on the respiratory system compared with the others. In addition, none of these molecules appear to have adverse effects on the kidneys, the heart or immune system, nor do they cause genetic mutations or cellular damage. The results also show that the substances **5d**, **5a**, and **5e** target Prostaglandin G/H Synthase 1, which is involved in inflammatory responses and could indicate a common mechanism of action or toxicity (**Table 9**).

Table 8. Excretion parameter prediction of the novel 1,3-di(1,3,4-oxadiazol-2-yl)benzene derivatives (**5a**, **5b**, **5c**, **5d** and **5e**).

Unit	Total clearance	Renal OCT2 substrate
	log mL/min/Kg	Categorical (Yes/No)
5d	0.216	No
5a	0.323	No
5b	0.13	No
5c	0.053	No
5e	0.276	Yes

Table 9. *In Silico* Toxicity Prediction of novel 1,3-di(1,3,4-oxadiazol-2-yl)benzene derivatives (**5a**, **5b**, **5c**, **5d** and **5e**).

	5d	5b	5c	5a	5e
LD₅₀ mg/Kg	2000 mg/Kg	888 mg/Kg	2035 mg/Kg	888 mg/Kg	1260 mg/Kg
Class	4	4	5	4	
Hepatotoxicity	Active	Active	Active	Active	Active
Neurotoxicity	Active	Active	Active	Active	Active
Nephrotoxicity	Inactive	Inactive	Inactive	Inactive	Inactive
Respiratory toxicity	Active	Active	Active	Inactive	Inactive
Cardiotoxicity	Inactive	Inactive	Inactive	Inactive	Inactive
Carcinogenicity	Active	Active	Active	Active	Active
Immunotoxicity	Inactive	Inactive	Inactive	Inactive	Inactive
Mutagenicity	Inactive	Inactive	Inactive	Inactive	Inactive
Cytotoxicity	Inactive	Inactive	Inactive	Inactive	Inactive
Possible toxicity targets	Prostaglandin G/H Synthase 1	-	-	Prostaglandin G/H Synthase 1	Prostaglandin G/H Synthase 1

3.5. Molecular dynamics study

3.5.1. Molecular Dynamics simulation for 50 ns

a. Root Mean Square Deviation (RMSD) Analysis

The RMSD graph illustrates the variation of the molecular structure with time, with the x-axis denoting time in nanoseconds (ns) and the y-axis indicating RMSD in nanometers (nm). Initially, there is a minor increase in RMSD, which is typical during system equilibration; however, at around 30 ns, the RMSD stabilizes at 0.25 nm, signifying a stable binding conformation of protein pancreatic α -amylase with compound **5d**, indicating low fluctuations and effective binding. Stability in molecular dynamics is essential for the inhibition of pancreatic α -amylase, as a stable RMSD value indicates robust binding and diminished flexibility, hence augmenting the inhibitory efficacy of compound **5d**. In comparison to the RMSD of the unbound enzyme or other inhibitors, this may suggest enhanced or equivalent efficacy. To further substantiate these findings, supplementary analyses including Root Mean Square Fluctuation (RMSF) for residue-specific movements analysis to verify critical active site interactions could be conducted.

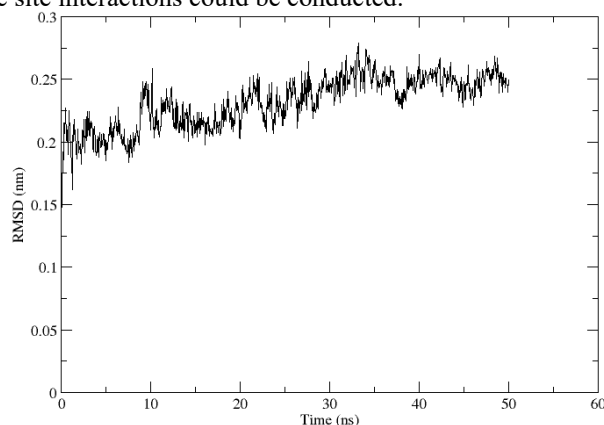


Fig. 5. Root Mean Square Deviation (RMSD) Analysis graphs as a function of time.

b. Root Mean Square Fluctuation (RMSF) Analysis

The RMS fluctuation (RMSF) graph provides insights into the flexibility of individual residues in the pancreatic α -amylase-compound 5d complex, where the x-axis represents residue index and the y-axis represents fluctuation in nanometers (nm). The RMSF profile shows that most residues exhibit low fluctuations, typically around 0.1–0.2 nm, indicating structural rigidity, and stable interactions. However, some residues, particularly those around residues 150–250 and 350–450, show significantly higher fluctuations, reaching up to 0.4–0.5 nm, which suggests regions with greater flexibility. These peaks often correspond to loop regions, active site residues, or binding pocket movements, which may play a role in ligand interaction and enzymatic activity. The low fluctuation of catalytic residues and the binding region suggests that compound 5d remains well-associated with pancreatic α -amylase, supporting its strong inhibitory potential. In contrast, high RMSF values in loop regions or solvent-exposed areas are expected, as they are naturally more flexible. To further validate these findings, Radius of Gyration (Rg) Plot can be performed to confirm the compound's interaction strength and its effect on the enzyme's dynamic behavior.

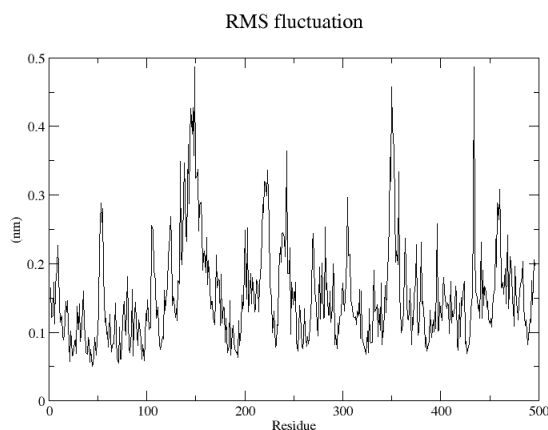


Fig. 6. Root Mean Square Fluctuation (RMSF) Analysis graph as a function of time.

c. Radius of Gyration (Rg) Plot

The radius of gyration (Rg) plot provides insights into the compactness and structural stability of the pancreatic α -amylase-5d complex over time. The x-axis represents simulation time in picoseconds (ps), while the y-axis represents Rg in nanometers (nm). The Rg values fluctuate between 2.25 nm and 2.3 nm, indicating that the overall structure maintains its compactness throughout the simulation. The absence of significant deviations suggests that the complex does not undergo major unfolding or destabilization upon ligand binding. A slight dip around 30 000 ps, followed by recovery, may suggest minor conformational adjustments, likely due to local rearrangements of flexible loops or the ligand binding-induced motion. However, since the fluctuations remain within a narrow range (~ 0.05 nm), it confirms that the binding of 5d does not cause large-scale unfolding or instability. To further validate these findings, hydrogen bonding analysis can be conducted to assess the structural impact of ligand 5d on pancreatic α -amylase and confirm its binding affinity.

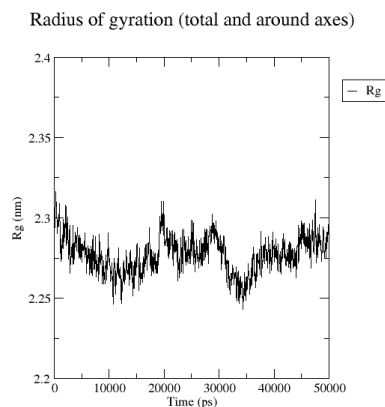


Fig 7. Radius of Gyration (Rg) Plot as a function of time.

d. Hydrogen Bonds:

The hydrogen bond (H-bond) analysis provides crucial insights into the stability and interaction strength of the pancreatic α -amylase-5d complex. The x-axis represents simulation time in picoseconds (ps), while the y-axis represents the number of hydrogen bonds. Throughout the simulation, the number of hydrogen bonds fluctuates between 340 and 400, with an average around 360–380, indicating a consistently strong hydrogen bonding network within the system. The absence of drastic drops suggests that the enzyme maintains its structural integrity while interacting with ligand 5d, supporting its potential as a stable inhibitor. Notably, minor fluctuations in hydrogen bonds are expected due to side-chain flexibility and solvent dynamics, but the overall consistency confirms that ligand 5d forms stable interactions with key residues in the active site of pancreatic α -amylase. This contributes to its strong binding affinity and inhibitory potential.

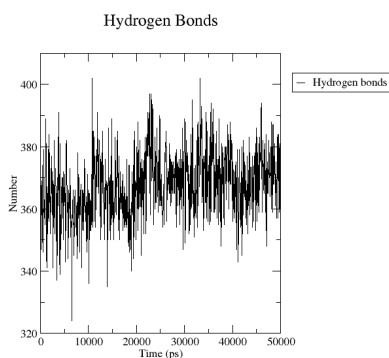


Fig. 8. Hydrogen Bonds graph as a function of time.

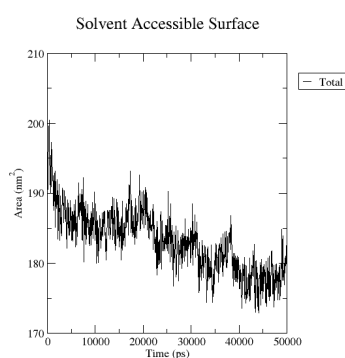


Fig. 9. Solvent Accessible Surface graph as a function of time.

e. Solvent Accessible Surface

The Solvent Accessible Surface Area (SASA) plot provides insights into the exposure of the pancreatic α -amylase-5d complex to the solvent, which is crucial for understanding protein folding, ligand binding, and overall structural stability. The x-axis represents simulation time in picoseconds (ps), while the y-axis represents SASA in nanometers squared (nm^2). Initially, the SASA value is around 200 nm^2 , but it gradually decreases and stabilizes around $175\text{--}185 \text{ nm}^2$, indicating a slight compaction of the protein structure over time. The reduction in SASA suggests that the binding of ligand 5d induces structural rearrangements, potentially leading to a more stable and less solvent-exposed conformation. This is a favorable characteristic, as decreased SASA often correlates with enhanced stability and stronger ligand-protein interactions. The gradual decline rather than sharp fluctuations further supports the notion that the complex remains stable without abrupt unfolding or major conformational changes. The final stabilized SASA value suggests that ligand 5d remains bound within the active site and does not significantly disrupt the overall protein structure.

3.5.2. Molecular Dynamics simulation for 100 ns

a. Root Mean Square Deviation (RMSD) Analysis:

RMSD measures the average deviation of the protein (or complex) atomic positions over time relative to a reference structure (commonly the starting conformation) (**Fig. 10**).

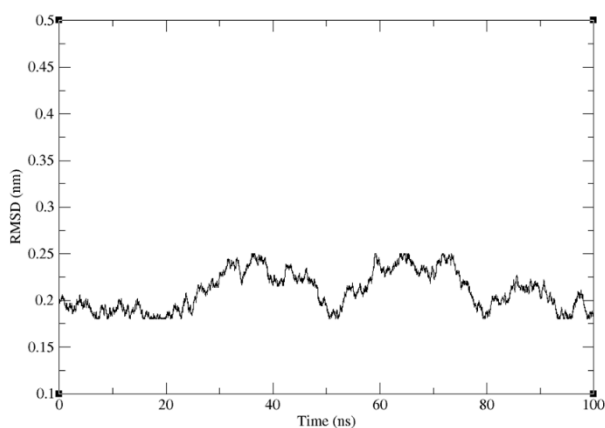


Fig 10. Root Mean Square Deviation (RMSD)

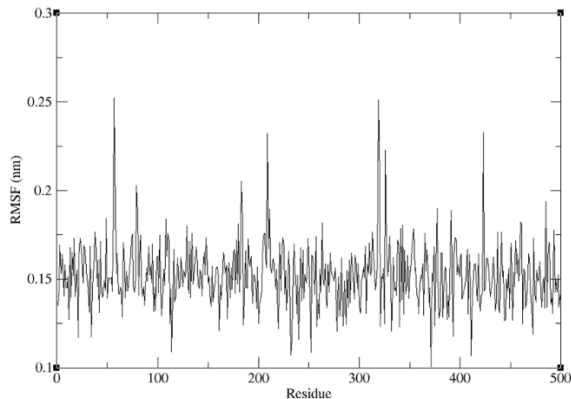


Fig. 11. Root Mean Square Fluctuation (RMSF) Analysis.

RMSD measures the average deviation of the protein atomic positions over time relative to a reference structure (commonly the starting conformation) (**Fig. 10**). In this simulation, the RMSD starts at approximately 0.10 nm at $t = 0$ ns and rises slightly to around 0.20 nm by ~ 25 ns. It then fluctuates mostly between 0.18 nm and 0.25 nm throughout the rest of the 100 ns simulation, with no persistent upward trend. A low and relatively stable RMSD after equilibration indicates that the protein maintains its overall structural integrity. The initial small increase corresponds to relaxation from the starting structure; the subsequent plateau and minor oscillations indicate that the system reached a stable conformational ensemble.

The RMSD does not show large continuous drift but exhibits small oscillations, suggesting local structural rearrangements without global unfolding. Occasional modest peaks (~ 0.25 nm, e.g., around 35 ns and 65 ns) may correspond to transient loop or side-chain movements. Consequently, the protein is structurally stable over the 100 ns simulation, with only minor fluctuations that are typical of thermal motion in solution.

b. Root Mean Square Fluctuation (RMSF) Analysis

RMSF measures per-residue positional fluctuations over the trajectory, usually with respect to the time-averaged structure (**Fig. 11**). It highlights flexible and rigid regions across residues. High RMSF values for a residue indicate greater flexibility (loops, termini, or mobile side chains). Low RMSF values identify stable secondary-structure elements (α -helices, β -sheets) and the rigid core. In this simulation, the majority of residues have RMSF values between 0.12 nm and 0.18 nm, indicating overall structural rigidity. Several peaks reaching ~ 0.26 – 0.28 nm are observed around residues ~ 60 , ~ 190 , ~ 300 , and ~ 380 , corresponding to more flexible loop regions or surface-exposed segments. The N-terminal residues (1–10) and C-terminal residues (~ 490 – 500) display moderately elevated fluctuations (~ 0.18 – 0.20 nm), which is expected due to terminal flexibility. The central structured core remains within 0.12–0.16 nm, indicating stable folding. The protein maintains a stable backbone with localized flexibility at loop regions. Peaks around residues ~ 190 and ~ 300 may correspond to functionally relevant flexible loops; further structural inspection could reveal roles in ligand access or conformational transitions. No major instability is observed, as the RMSF values remain below 0.30 nm throughout.

c. Radius of Gyration (Rg) Plot

The radius of gyration (Rg) analysis (**Fig. 12**) reveals that the protein maintains stable compactness, with Rg initially fluctuating around 2.25 nm before stabilizing at approximately 2.2 nm after 20,000 ps (20 ns), exhibiting minor fluctuations of ± 0.05 nm, which is typical for a folded protein under thermal motion. The absence of significant Rg increases or sudden drops suggests no major unfolding or structural collapse during the simulation. The stabilization of Rg aligns with potential RMSD trends, indicating that the system likely reached equilibrium after 20 ns.

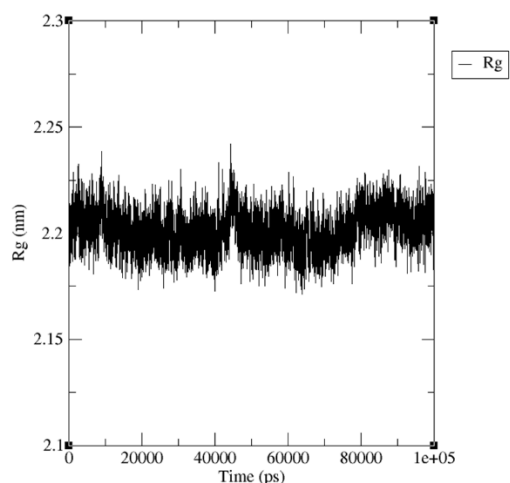


Fig 12. Radius of Gyration (Rg) Plot

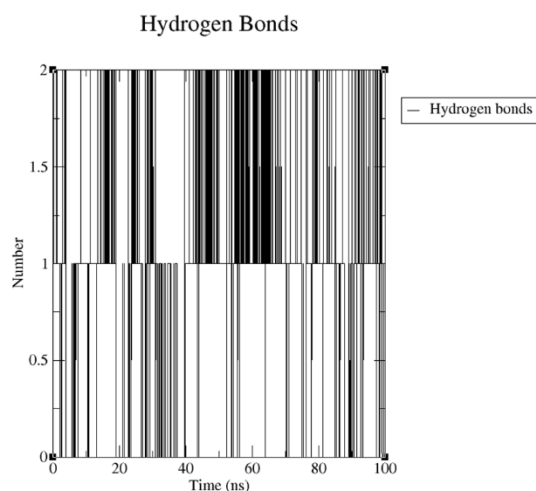


Fig. 13. Hydrogen Bonds Analysis

d. Hydrogen Bonds Analysis

The hydrogen bond analysis (**Fig. 13**) reveals dynamic yet stable interactions, with the total H-bond count fluctuating between 0.5 and 1.5 over the 100 ns simulation. While no persistent downward trend is observed, the low average H-bond count suggests transient interactions, which may reflect dynamic solvation or weak intra-protein/ligand contacts. Notably, the absence of high-occupancy H-bonds (e.g., $>50\%$ occupancy) implies no single dominant interaction stabilizes the structure, though collective weak bonds could still contribute to overall stability. When correlated with the earlier Rg and RMSD data where the protein maintained stable compactness (Rg ~ 2.2 nm) and equilibrium (RMSD plateau after 20 ns) the H-bond dynamics align with a flexible but globally folded system.

4. Conclusion

In conclusion, this study successfully synthesized and characterized new 1,3-di(1,3,4-oxadiazol-2-yl)benzene derivatives, which demonstrated promising antidiabetic potential through significant pancreatic α -amylase inhibition. Compound **5d** demonstrating the most potent activity, exhibiting inhibitions of 26.81%, 47.29%, and 72.61% at concentrations of 0.22, 0.45, and 0.9 mg/mL, respectively. Molecular docking studies further confirmed strong binding affinities of compounds **5d** (-124.7 Kcal/mol) and **5b** (-120.7 Kcal/mol) to the enzyme's active site. Moreover, compound **5d** exhibited favorable drug-likeness, bioavailability, and lower acute toxicity. Given the role of α -amylase in glucose metabolism, the significant inhibition observed underscores the therapeutic potential of these compounds in managing postprandial hyperglycemia. While the results are promising, further studies are needed to evaluate the long-term efficacy and safety of these compounds including *in vivo* models and clinical trials clinical settings.

CRedit author contribution

Assiya Atif: Methodology, Formal analysis, Validation, Writing - original draft. **Mohamed Marghich:** Formal analysis, Investigation, Software, Resources. **Nor Nabil:** Formal analysis, Software. **Abouelhaoul El Alami:** Writing – review & editing. **Nour Elhouda Daoudi:** Formal analysis, Investigation, Software, Resources. **Tarik Harit:** Software. **Fatima Youssoufi:** Writing – review & editing. **Mohammed Salah:** Conceptualization. **Abdelali Bitar:** Conceptualization, Validation, Supervision, Project administration. **Houssine Ait Sir:** Conceptualization, Methodology, Validation, Resources, Supervision, Project administration, Funding acquisition.

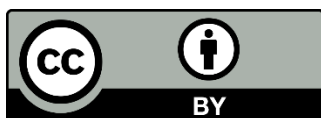
References

- [1] Tolba M. S., Kamal El-Dean A. M., Ahmed M., and Hassanien R. (2019) Synthesis, reactions, and biological study of some new thienopyrimidine derivatives as antimicrobial and anti-inflammatory agents. *J. Chin. Chem. Soc.*, 66 (5) 548-557.
- [2] Tolba M. S., Al-Hossainy A. F., Kamal Eldean A. M., and Younis O. (2022) From blue to green photoluminescence: design, synthesis, and DFT calculations of heterocyclic compounds containing chromenothienopyrimidine moiety. *Asian J. Org. Chem.*, 11 (3) e202100801.
- [3] El-Gaby M. S. A., Hussein M. F., Faraghally F. A., Drar A. M., and Gad M. A. (2023) Insecticidal activity and structure activity relationship study of some synthesized hydrazone, dihydropyridine and 3-cyano-1, 4-dihydro-pyridazin-4-one derivatives against *Aphis nerii*. *Curr Chem Lett*, 12 (3) 599-606.
- [4] Gad M. A., Bakry M. M., Tolba E. F., Alkhaibari A. M., Mashlawi A. M., Thabet M. A., Al-Taifi E. A., and Bakhite E. A. (2024) Exploration of some heterocyclic compounds containing trifluoromethylpyridine scaffold as insecticides toward *Aphis gossypii* insects. *Chem. Biodivers.*, 21 (6) e202400451.
- [5] Abd El-Lateef H. M., Khalaf M. M., Gouda M., Gad M. A., Abdelhamid A. A., Ismail A. F., Amer A. A., and Drar A. M. (2024) Synthesis and Insecticidal Evaluation of 3, 5-Dicyanopyridines Against Cotton Aphids via Microwave-Assisted Multicomponent Reactions. *Chem. Biodivers.*, 21 (4) e202400218.
- [6] Atif A., El Alami A., and Ait Sir H. (2025) Minireview of Synthesis Process of 1, 3, 4-Thiadiazole Derivatives. *Chem. Afr.*, 8 (7) 2663-2686.
- [7] Atif A., and Ait Sir H. (2025) Progress in the Synthesis of Tetrazoles. A Brief Review. *Org. Prep. Proced. Int.*, 1-16.
- [8] Al-Mulla A. (2017) A review: biological importance of heterocyclic compounds. *Der Pharma Chemica*, 9 (13) 141-147.
- [9] El-Ossaily Y., Alanazi N., Althobaiti I., Altaieb H., Al-Muailkel N., El-Sayed M., Hussein M. F., Ahmed I. M., Alnazi M. M., Fawzy A., Abdel-Raheem S. A. A., and Tolba M. (2024) Multicomponent approach to the synthesis and spectral characterization of some 3, 5-pyrazolidione derivatives and evaluation as anti-inflammatory agents. *Curr. Chem. Lett.*, 13 (1) 127-140.
- [10] Abdel-Raheem S. A., Fouad M. R., Gad M. A., El-Dean A. M. K., and Tolba M. S. (2023) Environmentally green synthesis and characterization of some novel bioactive pyrimidines with excellent bioefficacy and safety profile towards soil organisms. *J. Environ. Chem. Eng.*, 11 (5) 110839.
- [11] Sebaiy M. M., El-Adl S. M., Nafea A., Mattar A. A., Abdul-Malik M. A., Abdel-Raheem S. A., and Elbaramawi S. S. (2024) Review: Instrumental Analytical techniques for Evaluating some Anti-infective Drugs in Pharmaceutical Products and Biological Fluids. *Curr. Chem. Lett*, 13 (3) 491-502.
- [12] Gad M. A., Bakry M. M. S., Shehata E. A., and Dabour N. A. (2023) Insecticidal thioureas: Preparation and biochemical impacts of some novel thiobenzamide derivatives as potential eco-friendly insecticidal against the cotton leafworm, *Spodoptera littoralis* (Boisd.). *Curr. Chem. Lett*, 12 (4) 685-694.
- [13] El-Gaby M. S. A., Bakry M. M. S., Hussein M. F., Faraghally A. F., Khalil A. M., Gad M. A., and Drar A. M. (2023) Insecticidal efficacy and structure-activity relationship study of some synthesized cyanobenzylidene and bisbenzylidene derivatives against *Aphis nerii*. *Curr. Chem. Lett*, 12(3) 529-536.
- [14] Varala R., Kurra M., Amanullah M., Hussien M., and Alam M. M. (2024) Recent methods in the synthesis of chromeno [2, 3-d] pyrimidines. *Chem. Heterocycl. Compd.*, 60 (3) 111-117.

- [15] Chaban T. I., Klenina O. V., Chaban I. H., and Lelyukh M. I. (2024) Recent advances in the synthesis of thiazolo [4, 5-b] pyridines. Part 2: Focus on thiazole annulation to pyridine ring (microreview). *Chem. Heterocycl. Compd.*, 60 (3) 130-132.
- [16] Jasiński R. (2024) Synthesis of 1, 2-oxazine N-oxides via noncatalyzed hetero-Diels–Alder reactions of nitroalkenes (microreview). *Chem. Heterocycl. Compd.*, 60 (3) 121-123.
- [17] Thakur D., Kumar V., Tyagi S.K., and Parmar R.S., (2023) A Review on the Medicinal Significance of Heterocyclic Compounds. *Int. j. res. appl. sci. eng. technol.* 11 (6) 1-9.
- [18] Malek F., Harit T., Cherfi M., and Kim B. (2022) Insights on the synthesis of n-heterocycles containing macrocycles and their complexation and biological properties. *Molecules*, 27 (7) 2123.
- [19] Awasthi A., Rahman M. A., and Bhagavan Raju M. (2023) Synthesis, in silico studies, and in vitro anti-inflammatory activity of novel imidazole derivatives targeting P38 MAP kinase. *ACS omega*, 8 (20) 17788-17799.
- [20] Marinescu M. (2023) Benzimidazole-triazole hybrids as antimicrobial and antiviral agents: A systematic review. *Antibiotics*, 12 (7) 1220.
- [21] Khan S., Hussain R., Khan Y., Iqbal T., Chinnam S., Akif M., and Dera A. A. (2024) Hybrid benzothiazole derived fused triazole/thiazole derivatives as versatile anti-Alzheimer agents: Synthesis, characterization, biological evaluation and molecular docking studies. *J. Mol. Struct.*, 1318 (2024) 139200.
- [22] Cherfi M., Harit T., Amanchar M., Oulous A., and Malek F. (2024) An Overview of Pyrazole-Tetrazole-Based Hybrid Compounds: Synthesis Methods, Biological Activities and Energetic Properties. *Organics*, 5 (4) 575-597.
- [23] Cherfi M., Dib I., Harit T., Ziyat A., and Malek F. (2021) Synthesis and characterization of new pyrazole–tetrazole derivatives as new vasorelaxant agents. *Drug Dev. Res.*, 82 (7) 1055-1062.
- [24] Qadir T., Amin A., Sharma P.K., Jeelani I., and Abe H. (2022) A review on medicinally important heterocyclic compounds. *Open J. Med. Chem.*, 16 (1) e187410452202280
- [25] Baynes H. W. (2015) Classification, pathophysiology, diagnosis and management of diabetes mellitus. *J diabetesmetab*, 6 (5) 1-9.
- [26] Daoudi N. E., Bouziane O., Bouhrim M., and Bnouham M. (2022) Natural aldose reductase inhibitors for treatment and prevention of diabetic cataract: A review. *Herba Pol.*, 68 (1) 35-58.
- [27] Daoudi N. E., Bouhrim M., Bouziane O., Abdnim R., Bouknana S., Elrherabi A., Mekhfi H., Aziz M., Legssyer A., Ziyat A., and Bnouham M. (2023) Acute and Subchronic Treatment of Roasted and Unroasted Argan Oil on Postprandial Glycemia and Its Effect on Glucose Uptake by Isolated Rat Hemidiaphragm. *Lett. Drug Des. Discov.*, 20 (11) 1821-1829.
- [28] Marghich M., Daoudi N.E., Amrani O., Addi M., Hano C., Chen J.T., Mekhfi H., Ziyat A., Bnouham M., and Aziz M. (2022) Antioxidant Activity and Inhibition of Carbohydrate Digestive Enzymes Activities of *Artemisia campestris* L. *Front Biosci (Schol Ed)*, 14 (4) 25.
- [29] Tseng C. H. (2004) The potential biological mechanisms of arsenic-induced diabetes mellitus. *Toxicol. Appl. Pharmacol.*, 197 (2) 67-83.
- [30] Daoudi N.E., Bouhrim M., Ouassou H., Legssyer A., Mekhfi H., Ziyat A., Aziz M., and Bnouham M. (2020) Inhibitory effect of roasted/ unroasted *Argania spinosa* seeds oil on α - glucosidase, α -amylase and intestinal glucose absorption activities. *S. Afr. J.*, 135 (2020) 413-420.
- [31] Jayaraj S., Suresh S., and Kadeppagari R. K. (2013) Amylase inhibitors and their biomedical applications. *Starch-Stärke*, 65 (7-8) 535-542.
- [32] Atmaram U. A., and Roopan S. M. (2022) Biological activity of oxadiazole and thiadiazole derivatives. *Appl. Microbiol. Biotechnol.*, 106 (9) 3489-3505.
- [33] Sultana R., Ali A., Rana M., Ahmad I., Kamthan M., Almuqdad H. T. A., Mehandi R., Abid M., and El-Bahy Z. M. (2024) Synthesis of oxadiazole derivatives: Anti-bacterial, DNA binding and in silico molecular modelling approaches. *J. Mol. Struct.*, 1318 (2024) 139350.
- [34] Mendes Araujo H., de Moura G. A., Mendes Rocha Y., Viana Rodrigues J. P., and Nicolete R. (2023) Oxadiazole Derivatives as Anticancer and Immunomodulatory Agents: A Systematic Review. *Curr. Med. Chem.*, 30 (30) 3472-3485.
- [35] Veeramani V., Ganesh P. S. P., Bharanidharan S., Muthuraja P., Govindasamy C., and Rajamohan R. (2024) 2, 5-Disubstituted structures of 1, 3, 4-oxadiazole and 1, 3, 4-thiadiazole for anti-inflammatory potential: DFT approach for the structural aspects. *J. Mol. Struct.*, 1318 (2024) 139263.
- [36] Gupta O., Chawla G., and Pradhan T. (2024) 1, 3, 4-oxadiazole scaffold in antidiabetic drug discovery: an overview. *Mini-Rev. Med. Chem.*, 24 (20) 1800-1821.
- [37] Patidar M., Dubey R., Minz S., Pradhan M., and Deshmukh N. (2025) A mechanism-driven strategy for in-silico prediction, molecular docking, synthesis, and biological assessment of substituted 1, 3, 4-oxadiazole derivatives as novel antidiabetic agents. *J. Appl. Pharm. Res.*, 13 (2) 194-203.
- [38] Bhat N., Kumar A., Adiga M. C., and KR K. (2025) DESIGN, SYNTHESIS, AND ANTIDIABETIC EVALUATION OF SOME NEW COUMARIN-INCORPORATED 1, 3, 4-OXADIAZOLE-2-THIOL DERIVATIVES. *Rasayan J. Chem.*, 18 (2) 805-811

- [39] Hosangadi B.D., and Dave R.H. (1996) An efficient general method for esterification of aromatic carboxylic acids. *Tetrahedron Lett.*, 37 (35) 6375-6378.
- [40] I. Shekarchi M., Navidpour L., Khorami A. R., Partoazar A., Shafaroodi H., Rahmanipour N., and Shekarchi M. (2011) Synthesis of N-arylidene-2-(2-phenoxyphenyl) acetohydrazides as anti-inflammatory agents. *Iran. J. Pharm. Res.*, 10 (2) 369.
- [41] Galal S. A., Hegab K. H., Kassab A. S., Rodriguez M. L., Kerwin S. M., El-Khamry A. M. M. A., and El Diwani H. I. (2009) New transition metal ion complexes with benzimidazole-5-carboxylic acid hydrazides with antitumor activity. *Eur. J. Med. Chem.*, 44 (4) 1500-1508.
- [42] Rashid M., Husain A., Mishra R., Karim S., Khan S., Ahmad M., Al-wabel N., Husain A., Ahmad A., and Khan S. A. (2019) Design and synthesis of benzimidazoles containing substituted oxadiazole, thiadiazole and triazolo-thiadiazines as a source of new anticancer agents. *Arab. J. Chem.*, 12 (8) 3202-3224.
- [43] Atif A., Zahm S., Jebbari S., El Alami A., Youssoufi F., Ait Sir H., Kerraj S., and Salah, M. (2023) synthesis, admet, docking and molecular dynamics of new molecules derivatives from 1,3,4-oxadiazole and 1,3,4-bisoxadiazole: new compounds against hiv. *Eur. Chem. Bull.*, 12 (12) 4139 – 4156
- [44] Atif A., Ameer S., Bendaoud A., Hsissou R., Jebbari S., Ait Sir H., and Salah M. (2025) Comprehensive evaluation of a benzimidazole-1,3,4-oxadiazole derivative for corrosion protection of C38 steel in HCl: Experimental, molecular dynamics, monte carlo, and in silico pharmacokinetic approaches. *Curr. Chem. Lett.*, 14 (2025) 777-792
- [45] Yang J. M., and Chen C. C. (2004) GEMDOCK: a generic evolutionary method for molecular docking. *Proteins:Struct., Funct., Bioinf.*, 55 (2) 288-304.
- [46] Daina A., Michielin O., and Zoete V. (2017) SwissADME: a free web tool to evaluate pharmacokinetics, drug-likeness and medicinal chemistry friendliness of small molecules. *Sci. Rep.*, 7 (1) 42717.
- [47] Banerjee P., Eckert A. O., Schrey A. K., and Preissner R. (2018) ProTox-II: a webserver for the prediction of toxicity of chemicals. *Nucleic Acids Res.*, 46 (1) 257-263.
- [48] Pires D. E., Blundell T. L., and Ascher D. B. (2015) pkCSM: predicting small-molecule pharmacokinetic and toxicity properties using graph-based signatures. *J. Med. Chem.*, 58 (9) 4066-4072.
- [49] Amir M., and Shikha K. (2004) Synthesis and anti-inflammatory, analgesic, ulcerogenic and lipid peroxidation activities of some new 2-[(2, 6-dichloroanilino) phenyl] acetic acid derivatives. *Eur. J. Med. Chem.*, 39 (6) 535-545.
- [50] Li D. J., Dan F. J., and Fu H. Q. (2008) Synthesis and antibacterial activities of 1, 3-bis [3-n-acetyl-2-aryl-1,3,4-oxadiazoline-5-yl] benzenes. *Heterocycl. Commun.*, 14 (1-2) 101-106.
- [51] Atif A., El Alami A., Youssoufi F., Jebbari S., and Ait Sir H. (2025) Review of synthesis process of 1,3,4-oxadiazole analogs. *Curr. Chem. Lett.*, 14 (2025) 339–364
- [52] Atif A., Ameer S., and Ait Sir H. (2025) Synthesis, characterization and in silico evaluation of 2,5-bis(2-(trifluoromethyl)-1Hbenzimidazol-5-yl)-1,3,4-oxadiazole: Reactivity, ADME/toxicity, and docking against therapeutic targets. *Curr. Chem. Lett.*, 14 (2025) 793-804
- [52] Jha K. K., Samad A., Kumar Y., Shaharyar M., Khosa R. L., Jain J., Kumar V., and Singh P. (2010) Design, synthesis and biological evaluation of 1, 3, 4-oxadiazole derivatives. *Eur. J. Med. Chem.*, 45 (11) 4963-4967.
- [53] Jakopin Z., and Dolec M. S. (2008) Recent Advances in the Synthesis of 1, 2, 4-and 1, 3, 4-Oxadiazoles. *Curr. Org. Chem.*, 12 (10) 850-898.
- [54] Yadav D., Bodke S., Biradar A., and Kenchappa R. (2016) Synthesis, characterization and biological evaluation of 2-(2-substituted)-5-phenyl-1, 3, 4-oxadiazole and 3, 6-diphenyl [1, 2, 4] triazole [3, 4][1, 3, 4] thiadiazole derivatives. *Ind J Adv Chem Sci.*, 4 (2016) 269-275.
- [55] Kaur N., Kumar V., Nayak S. K., Wadhwa P., Kaur P., and Sahu S. K. (2021) Alpha-amylase as molecular target for treatment of diabetes mellitus: A comprehensive review. *Chem. Biol. Drug Des.*, 98 (4) 539-560.
- [56] Nawaz M., Taha M., Qureshi F., Ullah N., Selvaraj M., Shahzad S., Chigurupati S., Waheed A., and Almutairi F. A. (2020) Structural elucidation, molecular docking, α -amylase and α -glucosidase inhibition studies of 5-amino-nicotinic acid derivatives. *BMC chem.*, 14 (1) 1-11.
- [57] Altaff S. M., Raja Rajeswari T., and Subramanyam, C. (2020) Synthesis, α -amylase inhibitory activity evaluation and in silico molecular docking study of some new phosphoramidates containing heterocyclic ring. *Phosphorus Sulfur Silicon Relat. Elem.*, 196 (4) 389-397.
- [58] Khirallah S. M., Ramadan H. M., Aladl H. A. A., Ayaz N. O., Kurdi L. A., Jaremko M., Alshawwa S. Z., and Saied E. M. (2022) Antidiabetic potential of novel 1, 3, 5-trisubstituted-2-thioxoimidazolidin-4-one analogues: Insights into α -glucosidase, α -amylase, and antioxidant activities. *Pharmaceuticals*, 15 (12) 1576.
- [59] Saddique F. A., Ahmad M., Ashfaq U. A., Muddassar M., Sultan S., and Zaki M. E. (2022) Identification of cyclic sulfonamides with an N-arylacetyl group as α -glucosidase and α -amylase inhibitors: biological evaluation and molecular modeling. *Pharmaceuticals*, 15 (1) 106.
- [60] Harit T., Cherfi M., Elhouda Daoudi N., Isaad J., Bnouham M., and Malek F. (2022) Hybrid Pyrazole-Tetrazole Derivatives with High α -Amylase Inhibition Activity: Synthesis, Biological Evaluation and Docking Study. *ChemistrySelect*, 7 (48) e202203757.

- [61] Qian M., Haser R., Buisson G., Duee E., and Payan F. (1994) The Active Center of a Mammalian. α -Amylase. Structure of the Complex of a Pancreatic. α -Amylase with a Carbohydrate Inhibitor Refined to 2.2- Å Resolution. *Biochemistry*, 33 (20) 6284-6294.
- [62] Gupta S., Baweja G. S., Gupta G. D., and Asati V. (2023) Identification of potential N-substituted 5-benzylidenethiazolidine-2, 4-dione derivatives as α -amylase inhibitors: Computational cum synthetic studies. *J. Mol. Struct.*, 1287 (2023) 135596.
- [63] Zala A. R., Naik H. N., Ahmad I., Patel H., Jauhari S., and Kumari P. (2023) Design and synthesis of novel 1, 2, 3-triazole linked hybrids: Molecular docking, MD simulation, and their antidiabetic efficacy as α -Amylase inhibitors. *J. Mol. Struct.*, 1285 (2023) 135493.
- [64] Oulous A., Cherfi M., Daoudi N.E., Harit T., Yahyi A., Bnouham M., and Malek F. (2024) Synthesis, characterization and α -amylase inhibition activity of new family of tetrapodal ligands with pyrazole-tetrazole subunits. *J. Mol. Struct.* 1321 (2025) 140254
- [65] Knoll K. E., van der Walt M. M., and Loots D. T. (2022) In silico drug discovery strategies identified ADMET properties of decoquinatone RMB041 and its potential drug targets against *Mycobacterium tuberculosis*. *Microbiol. Spectr.*, 10 (2) e02315-21.



© 2026 by the authors; licensee Growing Science, Canada. This is an open access article distributed under the terms and conditions of the Creative Commons Attribution (CC-BY) license (<http://creativecommons.org/licenses/by/4.0/>).